



## Early View

Original article

# Comparison of histologic and computed tomographic measurements of pig lung bronchi

Volker H. Schmitt, Christine Schmitt, David Hollemann, Andreas Mamilos, Willi Wagner, Oliver Weinheimer, Christoph Brochhausen

Please cite this article as: Schmitt VH, Schmitt C, Hollemann D, *et al.* Comparison of histologic and computed tomographic measurements of pig lung bronchi. *ERJ Open Res* 2020; in press (<https://doi.org/10.1183/23120541.00500-2020>).

This manuscript has recently been accepted for publication in the *ERJ Open Research*. It is published here in its accepted form prior to copyediting and typesetting by our production team. After these production processes are complete and the authors have approved the resulting proofs, the article will move to the latest issue of the ERJOR online.

Copyright ©ERS 2020. This article is open access and distributed under the terms of the Creative Commons Attribution Non-Commercial Licence 4.0.

## Original article

### Comparison of histologic and computed tomographic measurements of pig lung bronchi

Volker H. Schmitt<sup>1,2\*</sup>, Christine Schmitt<sup>3\*#</sup>, David Hollemann<sup>4</sup>, Andreas Mamilos<sup>5</sup>, Willi Wagner<sup>6,7</sup>, Oliver Weinheimer<sup>6,7§</sup>, Christoph Brochhausen<sup>5,8§</sup>

<sup>1</sup>Department of Cardiology, University Medical Centre, Johannes Gutenberg University of Mainz, Mainz, Germany

<sup>2</sup>German Center for Cardiovascular Research (DZHK), Partner Site Rhine Main, Mainz, Germany

<sup>3</sup>Practice Dr. Wolf and Colleagues, Mainz, Germany

<sup>4</sup>Institute of Clinical and Molecular Pathology, State Hospital Horn, Horn, Austria

<sup>5</sup>REPAIR-lab, Institute of Pathology, University of Regensburg, Regensburg, Germany

<sup>6</sup>Department of Diagnostic and Interventional Radiology, University Hospital Heidelberg, Heidelberg, Germany

<sup>7</sup>Translational Lung Research Centre Heidelberg (TLRC), German Lung Research Centre (DZL), Heidelberg, Germany

<sup>8</sup>Central Biobank Regensburg, University Regensburg and University Hospital Regensburg, Regensburg, Germany

\*Both authors contributed equally to this work and share first authorship

#This work contains parts of the MD thesis of C. Schmitt

§Both authors contributed equally to this work and share senior authorship

Corresponding author:

Prof. Dr. Christoph Brochhausen

REPAIR-lab, Institute of Pathology

European Institute of Excellence for Tissue Engineering & Regenerative Medicine

University of Regensburg

Franz-Josef-Strauß Allee 11

93053 Regensburg, Germany

Tel.: ++49 0941 944 6636

e-mail: [christoph.brochhausen@ukr.de](mailto:christoph.brochhausen@ukr.de)

## **Summary of take home messages**

Automated measurement techniques advance diagnostics of lung diseases. Pig bronchi wall size varied between MicroCT, CT IBM, CT FWHM and histology. CT IBM was closest to histologic results followed by MicroCT. CT FWHM highly differed to all other groups.

## **Abstract**

**Aim:** Light microscopy is used as template in the evaluation and further development of medical imaging methods. Tissue shrinkage caused by histological processing is known to influence lung tissue dimensions. In diagnostic of chronic obstructive pulmonary disease, computed tomography (CT) is widely used for automated airway measurement. We compared the bronchus wall thickness in histological and different image analysis methods.

**Methods:** Airway measurements of pig lungs were performed after freezing under controlled inflation pressure in a liquid nitrogen bath. The wall thickness of seven bronchi was measured via MicroCT and CT using the integral based method (IBM) and the full-width-at-half-maximum method (FWHM) automatically and histologically on frozen and paraffin sections. Statistical analysis was performed using the Wilcoxon test, Pearson's correlation coefficient with a significance level at  $P < 0.05$ , scatter plots and Bland Altman plots.

**Results:** Bronchus wall thickness was smallest in frozen sections (median 0.71 mm) followed by paraffin sections (median 0.75 mm), MicroCT (median 0.84 mm) and CT measurements using IBM (median 0.68 mm) and FWHM (median 1.69 mm). Statistical significant differences were found among all tested groups ( $p < 0.05$ ) except for CT IBM and paraffin and frozen sections and MicroCT. High correlation was present between all parameters with statistical significance ( $p < 0.05$ ).

**Conclusions:** Significant differences in airway measurement were found in the different analyzing methods. The absolute measurements with CT IBM were closest to the histological results followed by MicroCT, whereas CT FWHM revealed a distinct divergence to the other groups.

## Introduction

Imaging procedures such as sonography, x-ray radiography, computed tomography (CT) and magnetic resonance imaging (MRI) represent integral diagnostic routes and play a crucial role in clinical science. In the evaluation of imaging techniques the correlation to light micrographs of histological slides is a commonly used method and crucial to assess the genuineness of the medical image compared to the original object *in vivo* [1-3]. Exemplarily, in the development of ultrasonic carotid artery wall thickness measurement and its implementation into clinical use the accuracy and interpretation of sonographic measurements gathered in epidemiological studies and clinical trials were verified via ultrasonic-pathologic comparison by correlating ultrasound data against histological measurements of cadavers *in vitro* and *in situ* [1, 2]. Interestingly, the histologic specimens in these studies were already corrected for shrinkage due to histologic processing [1, 2]. Also in CT the ability of appropriate sizing plays a decisive role. An appropriate example is given by the CT evaluation of renal masses [4], where appropriate sizing in imaging techniques is a matter of discussion since studies exist showing a relevant discrepancy between radiologic and pathologic measurements with overestimation of tumor size in CT measurement [5]. This has relevant implications for pre-operative patient management regarding prognosis [6] and, in renal surgery, discrepancies in measuring methods even affect decisions on nephron-sparing surgery in certain patients [7].

In thoracic radiology, CT technology has become indispensable [8], especially the automatized assessment of airway geometry derived from high resolution CT scans are of great importance in diagnostics and surveillance of pulmonary diseases [9]. Since various lung diseases are accompanied with an increase in airway wall thickness due to airway remodeling [10-12], which is based on changes in the airway structure including subepithelial fibrosis, increased smooth muscle mass, submucosal gland enlargement, revascularization and epithelial alterations [13], qualitative and quantitative analyses of CT images of the lungs are becoming increasingly important not only for the better understanding of lung disease mechanisms and drug targeting strategies but also in the medical and surgical management of these patients [14-16]. Kosciuch *et al.* demonstrated a significant correlation between small airway wall thickness and lung function measured via spirometry in patients with bronchial asthma and chronic obstructive pulmonary disease (COPD). This group found increased air trapping in asthma to be reflected by the thickening of the airway wall and elevated airway resistance and responsiveness as a result of airway thickening in COPD [11]. Thus, asthma and COPD can be differentiated via airway dimension measurement in high resolution CT

since the bronchial walls in asthmatic patients are thicker than in subjects with COPD, whereas airway diameter in asthma seems to be smaller than in COPD [17]. In both diseases, the airway wall thickness and the lumen diameter are related to disease severity. The airway wall thickness measured in high resolution CT images was shown to correlate with functional parameters of airflow obstruction in COPD patients. Moreover, it was demonstrated that the bronchial wall thickness in smokers was significantly higher than in non-smokers [18]. In COPD the bronchial dimensions were shown to depend on the smoking status and smoking-induced airway remodeling was partially reversible after smoking cessation even in long-term heavy smokers [19]. Further, it was demonstrated that short-time airway geometry changes can be detected in severe COPD with quantitative CT [20]. Therefore, huge efforts have been made to develop radiological measurement methods using CT, such as non-invasive 3D measurements and quantifications of airway geometry and lung parenchyma aiming to advance diagnostic and prognostic methodologies for several diseases like asthma, emphysema, COPD and cystic fibrosis [10-12, 21-24]. Several high resolution techniques exist such as synchrotron radiation-based CT, which allows the *in vivo* study of regional lung ventilation in mice and high resolution lung imaging on human scale [25], as well airway function measurements by direct quantification of stable Xenon gas inserted as an inhaled contrast agent using K-edge subtraction imaging and the dynamics of Xenon wash-in can be used to calculate quantitative maps of regional specific lung ventilation [16]. Spiral-CT opens the possibility of acquiring 3D images of the pulmonary bronchial tree and gives access to quantitative measurements of regional lung volume, ventilation and mechanical properties [16]. Micro-CT represents a promising technique in non-destructive 3D imaging and morphometric analysis with almost microscopic resolution and sufficient soft tissue contrast and opens further possibilities in the assessment of lung micro-architecture [26]. However, conventional methods rely on a large gray value contrast between lung and surrounding tissues and fail on scans with lungs that contain dense pathologies [27]. Also, accurate determination of inner and outer airway wall surfaces of a complete 3D tree structure is challenging because of its complex nature [9]. Moreover, the assessment of thin structures like airway walls causes difficulties in the measurement of the density and the thickness of these structures due to the limited spatial resolution of clinical CT scanners [10]. Therefore, different CT measurement techniques exist like the full-width-at-half-maximum method (FWHM) and the more advanced integral based method (IBM). FWHM is thought to overestimate the thickness of bronchus walls and IBM was developed with the intent to more accurately approach the true anatomic size [10].

In the further development and evaluation of lung imaging methods the comparison of radiologic images and radiologic measurements of the airway with histologic slides is a necessary tool. However, volume alteration of tissue due to fixation and histologic processing is a well-known phenomenon in surgical pathology [28-30] and has also been described in lung tissue [31-40]. As a consequence, in the assessment and further development of imaging techniques and radiologic methods it is also crucial to investigate the histologic correlate to which these procedures are compared to - with the aim of discovering the histologic procedure, which qualifies best for reflecting the *in vivo* structure most accurately. Hence, it is necessary to assess the fixation and processing induced volume alteration in a tissue type when it shall be used as a template for imaging procedures. Overall, the histologic method which best reflects the *in vivo* situation supposedly should be assessed for each tissue. In the present study, for the first time, measurements of the bronchus wall thickness were compared between paraffin and frozen sections as well as MicroCT and the two CT methods IBM and FWHM.

## **Materials and Methods**

The present study was performed with four pig lungs. Since two of these were gained from another animal study and the two remaining lungs were obtained from the local abattoir immediately after slaughtering no animals were killed for the sole purpose of this study. The experimental method used in this investigation was already described in detail elsewhere [40, 41]. In brief, four excised pig lungs were intubated using a conventional tracheal tube (Willy Rüschi GmbH, Kernen, Germany) and frozen in liquid nitrogen (temperature  $-183^{\circ}\text{C}$ ) in ventilated condition when visually inflated to total lung capacity by use of a mechanical ventilator (SV 900, Siemens-Elema AB, Sweden) with a positive end expiratory pressure set to 20 mmHg. The frozen lungs were given in a box which was partly filled with curd to optimize stabilization for later cutting and was subsequently given into the liquid nitrogen bath again. This compound was scanned with a routine chest CT examination protocol (Brilliance 16, Philips Medical Solutions, Leiden, Netherlands, tube voltage – 120 kV, tube current – 120 mAs, slice thickness – 1.0 mm, increment – 0.8 mm, kernel D). The used clinical CT scanner underwent dedicated routine calibration for water every three months and for air daily, also the MicroCT scanner was calibrated to the Hounsfield scale routinely. Immediately after CT image reconstruction, optimal localizations where bronchi crossed the image plane perpendicularly were marked with ink and wire by helps of the CT gantry's laser light. Guided by these marks the boxes were cut using an anatomical saw (Selekta 3, Mado,

Dornhan/Blackforest, Germany) and slices with correlating bronchi were selected based on macroscopic and CT image examination. Small cuboids containing the selected bronchi were prepared. These cuboids were scanned with a desktop cone-beam Micro-CT scanner (SCANCO Medical,  $\mu$ CT 40) with an isotropic spacing of 0.02 mm. Afterwards, of these cuboids, frozen sections of 5  $\mu$ m thickness were performed using a cryomicrotome and stained with hematoxylin and eosin (HE) according to standard protocols. On the remaining tissue the surface of the cutting edge was marked and the specimens were fixed in 4% formalin for at least 12 hours under room temperature. Then, paraffin sections of exactly the same cutting edge as the frozen sections were performed and stained with HE. Exclusion of specimens occurred once the bronchi could not be microscopically and computertomographically correlated or due to missing intactness of anatomic structures, e.g. lack of the entire intact bronchial wall including the epithelium. So, in the end, only exactly and perfectly preserved bronchus specimens were used. After this rigorous selection procedure, a total of 7 bronchi remained for further evaluation (**Figure 1**). Histological investigation and measurement were performed using a light microscope (BX45, Olympus, Hamburg, Germany) and microscope software (Cell sense entry, Olympus, Hamburg, Germany). The optical system of the microscope underwent calibration yearly during the routine service performed by the manufacturer. Digital Images were taken with a microscope camera (Olympus SC30, Olympus, Hamburg, Germany). From the chosen bronchi one frozen and one paraffin section were analysed, in each slide the wall thickness of the bronchus was investigated using high power fields (hpf) of 400-fold magnification. For every bronchus 40 measurements were implemented at different positions of the bronchus wall in both the paraffin and the frozen section, as previously described [40]. The corresponding CT measurements were performed using the scientific software system YACTA (yet another CT analyser, version 1.1.4.1), as described in detail before [10]. The grey scale profile across the airway wall was detected by 256 centrifugal rays. The integral-based method was used to quantify the median airway wall thickness. The wall thickness was determined in areas where the bronchus was surrounded by parenchyma. Localizations which could not be reasonably assessed by the grey scale profile, e.g. when the airway wall was attended by bronchial arteries, were automatically excluded. Data collection occurred using Microsoft Excel (Microsoft Excel 2010, Microsoft Corporation, Redmond, WA, USA) and statistical analyses was conducted with SPSS Statistics 20 (IBM Deutschland GmbH, Ehningen, Germany). Wilcoxon test and Pearson's correlation coefficient were performed with a significance level at 0.05 and scatter plots as well as Bland Altman plots were conducted.

## Results

The thickness of the pig bronchus walls was smallest when measured by CT using IBM (median 0.68 mm, mean 0.72 mm, minimum of 0.43 mm, maximum of 0.9 mm) followed by measurement in frozen sections (median 0.71 mm, mean 0.66 mm, minimum 0.42 mm, maximum of 0.83 mm) and paraffin sections (median 0.75 mm, mean 0.75 mm, minimum 0.05 mm, maximum 0.91 mm). Bronchus wall thickness measured with Micro-CT amounted to 0.84 mm at the median (mean 0.82 mm, minimum 0.56 mm, maximum of 0.95 mm). CT measurement using FWHM resulted in the highest wall thickness with the largest distance to the other groups (median 1.69 mm, mean 1.64 mm, minimum 1.36 mm, maximum 1.77 mm). The results are summarized in **Table 1** and **Figure 2**. Wilcoxon test with a significance level at  $p < 0.05$  revealed statistical significance for all groups except for CT using IBM and paraffin section ( $p = 0.237$ ), frozen sections ( $p = 0.176$ ) as well as MicroCT ( $p = 0.063$ ) (**Supplement Table 1**) [40].

Pearson's correlation coefficient revealed high correlation between all groups and for all statistical significance was present. The highest correlation was found between MicroCT and CT using FWHM [ $R = 0.929$  (95%CI 0.046; 0.994),  $p = 0.003$ ], followed by paraffin and frozen sections [ $R = 0.902$  (95%CI 0.638; 0.988),  $p = 0.005$ ] as well as paraffin sections and MicroCT [ $R = 0.902$  (95%CI 0.309; 0.997),  $p = 0.005$ ]. High correlation was also present between MicroCT and CT using IBM [ $R = 0.898$  (95%CI 0.721; 0.988),  $p = 0.006$ ], frozen sections and CT using FWHM [ $R = 0.866$  (95%CI 0.240; 0.981),  $p = 0.012$ ], paraffin sections and CT using IBM [ $R = 0.860$  (95%CI 0.291; 0.995),  $p = 0.013$ ], frozen sections and MicroCT [ $R = 0.813$  (95%CI 0.169; 0.994),  $p = 0.026$ ], paraffin sections and CT using FWHM [ $R = 0.811$  (95%CI -0.243; 0.989),  $p = 0.027$ ] as well as frozen sections and CT using IBM [ $R = 0.805$  (95%CI 0.146; 0.987),  $p = 0.029$ ]. The smallest correlation, which still was high, was present between CT using IBM and CT using FWHM [ $R = 0.794$  (95%CI -0.151; 0.991),  $p = 0.033$ ] (**Table 2** and **Supplement Table 2**). These results are illustrated by regression plots in **Figure 3**, **Figure 4** and **Supplement Figure 1**.

Mean differences and limits of agreement in accordance with the approach of Bland and Altman were calculated between all groups. The smallest mean difference was found between CT IBM and the paraffin sections with 0.034 mm, the agreement limits ranged from -0.148 mm to 0.217 mm. The largest mean difference was found between CT FWHM and the frozen sections with -0.989 mm and agreement limits ranging from -1.134 mm to -0.844 mm.

The Bland Altman plots are shown in **Figure 5**, **Figure 6** and **Supplement Figure 1**, the mean differences between all groups are summarized in **Supplement Table 3**.

Altogether, the present results revealed close measurements of bronchial walls in paraffin and frozen sections which differed significantly but revealed a high correlation between the two methods (median paraffin sections 0.75 mm, median frozen sections 0.71 mm, divergence of median values 0.04 mm, relative divergence 5%, Wilcoxon  $p = 0.018$ ,  $R = 0.902$ ,  $p = 0.005$ ). CT using IBM presented the measurements which were closest to the results of the histological data with a slight underestimation of the bronchial wall thickness compared to paraffin and frozen sections (median CT IBM 0.68 mm, divergence to median paraffin sections 0.07 mm, relative divergence to paraffin sections 9.3%, divergence to median frozen sections 0.03 mm, relative divergence to frozen sections 4.2%). Wilcoxon test revealed no significant difference [ $p = 0.237$  (paraffin sections),  $p = 0.176$  (frozen sections)] to the two histological methods, and simultaneously correlation was high to both groups (paraffin sections and CT IBM:  $R = 0.860$ ,  $p = 0.013$ ; frozen sections and CT IBM:  $R = 0.805$ ,  $p = 0.029$ ). The difference of MicoCT measurements to histology differed by 12.0% to paraffin sections and by 18.3% to frozen sections (median MicroCT 0.84 mm, divergence to median paraffin sections 0.09 mm, relative divergence to paraffin sections 12.0%, Wilcoxon  $p = 0.043$ ,  $R = 0.902$ ,  $p = 0.005$ ; divergence to median frozen sections 0.13 mm, relative divergence to frozen sections 18.3%, Wilcoxon  $p = 0.018$ ,  $R = 0.813$ ,  $p = 0.026$ ). CT using FWHM (median 1.69 mm) revealed a considerable difference to the results of the other methods. Compared to histology, there was a divergence of 125.3% to paraffin sections (divergence to median paraffin sections 0.94 mm, relative divergence 125.3%, Wilcoxon  $p = 0.018$ ,  $R = 0.811$ ,  $p = 0.027$ ) and 138.0% to frozen sections (divergence to median frozen sections 0.98 mm, relative divergence 138.0%, Wilcoxon  $p = 0.018$ ,  $R = 0.866$ ,  $p = 0.012$ ). The difference of CT using FWHM to MicroCT was 0.85 mm (relative divergence 101.2%, Wilcoxon  $p = 0.018$ ) with a high correlation of the measurements of both groups ( $R = 0.929$ ,  $p = 0.003$ ). The highest difference of all assessed groups was present in the divergence between the two CT methodologies IBM and FWHM, which amounted the highest difference of all assessed groups (median CT IBM 0.68 mm, median CT FWHM 1.69 mm, absolute divergence 1.01 mm, relative divergence 148.5%, Wilcoxon  $p = 0.018$ ,  $R = 0.794$ ,  $p = 0.033$ ). An overview of absolute and relative median differences between all groups is given in **Supplement Table 4**.

## **Discussion**

The present study represents the first comparing analysis of different histologic and radiologic methods, namely paraffin and frozen sections, Micro-CT and CT including the two CT approaches IBM and FWHM, in the quantitative assessment of the airway structure by measuring the bronchus wall thickness of pig bronchi. The difference between paraffin and frozen sections amounted 5%. CT using IBM revealed the measures closest to histology with a divergence of 4.2% to frozen and 9.3% to paraffin sections. Interestingly, no statistically significant difference but a high and significant correlation was present between CT using IBM and both histological methods. The measurements of MicroCT and CT with IBM differed by 19.0%. Interestingly, the two CT methods FWHM and IBM revealed the highest divergence of all groups (148.5%). By this, while the measurements of CT using IBM only differed slightly from histology (9.3% and 4.2%, respectively) and MicroCT (19%), a large difference was present between all groups and CT using FWHM (divergence of 125.3% to paraffin and of 138% to frozen sections, divergence of 101.2% to MicroCT). These differences were statistically significant and revealed a high correlation. The divergence of MicroCT to histology was 12.0% (paraffin sections) and 18.3% (frozen sections).

The diagnostic assessment of the airway wall by CT offers the advantage of minimal invasiveness and thus has become a useful and authentic tool for airway imaging [13] to enhance understanding and diagnostics of several lung diseases [11, 15, 17, 18]. For accurate airway quantification several methods are being tested and are subject to continuous further development [9, 42]. To assess and advance imaging techniques it is necessary to compare radiologic image data to histologic data [43] as shown in several developments like carotid artery sonography [1, 2] and mammography [44] or even to expose limited usefulness of radiologic methodologies as shown in the assessment of optic nerve invasion of retinoblastoma [45] and the characterization of adnexal masses [46]. In diagnosing lung diseases like pulmonary adenocarcinomas, CT assessment represents a useful aid in determining the best surgical method [47] by measurement of the tumor size [48]. However, volume alteration caused by fixation and processing which also occurs in lung tissue [31-39] evokes the need to investigate the volume alterations due to histologic tissue processing. In this context, a comparison of lung adenocarcinoma assessment by CT and gross pathology measurements revealed a statistically significant difference between the mean CT and mean pathology measurement of 18.3% [49]. The results of the present study revealed considerable differences in bronchial wall measurements between histology and CT. These findings are in line with previous investigations in the literature. In a study by Isaka *et al.* the tumor size of lung adenocarcinoma depicted by CT and the measurements performed by the surgical

pathologist were compared and significantly smaller lung tumor sizes in macroscopic measurement as well as in paraffin and frozen sections were found compared to CT data [50]. In detail, the specimens were macroscopically already significantly smaller compared to the radiologic data but the most considerable loss in size was seen after histologic processing. Interestingly, in contrast to the results of the present study concerning the bronchus wall, in the investigation by Isaka *et al.* the tissue size in paraffin sections was slightly smaller than in frozen sections [50]. Multiple reasons for possible tissue shrinkage exist in the context of fixation and histologic processing like exposition to air [30, 51], fixation in alcohol, formalin [52] or formaldehyde [53, 54], freezing [55], embedding in paraffin, cutting and stretching [54]. However, the dimension of volume loss was shown to vary with tissue type, specimen size, used fixatives, and tissue processing method [30, 56]. In their study Isaka *et al.* assumed the discordance observed between CT measured tumor size and light microscopic tumor size to be due to shrinkage of the lepidic component in the tumor [50]. Regarding the present results, unlike lung adenocarcinoma the size of the bronchial wall thickness was smaller in frozen than in paraffin sections. This might be caused by the different tissue structure of the airway compared to a solid soft tissue tumor like lung adenocarcinoma, which contains also a considerable amount of cartilage tissue and therefore may underlie other shrinkage properties than soft tissue. Since besides evaluating imaging methods in biomedical research the comparison of image features with corresponding histopathology represents the current gold standard for disease assessment [37], knowledge about fixation and processing induced tissue shrinkage is crucial for the particular assessed tissue type, especially when samples are compared after different processing procedures [57]. The results of the present study revealed frozen sections and CT using IBM to match best and CT using FWHM to differ most in size from other radiologic as well as histologic data. However, the review of the literature makes clear that each of the used methods in former and the present study might reveal different measurements compared to the *in situ* situation in the body. Therefore, the impact of size differences of bronchial structure between paraffin and frozen sections has to be further investigated and further studies are required to assess which histologic method represents the *in vivo* size proportion of the bronchial wall best. In addition, it is a matter of fact that the extent of tissue shrinkage depends on the several processing parameters such as fixation agent and concentration. This is the reason why results should be interpreted in the context of the procession methods. Knowledge about volume alteration due to fixation and processing together with the further development and improvement of medical imaging methods is crucial since differences between radiologic and pathologic tissue volumes could have

considerable implications in the treatment and prognosis of patients [49]. Furthermore, regarding the lung, tissue shrinkage due to fixation, embedding and staining was shown to vary considerably among mammalian species revealing the necessity of assessing these volume changes in different species, particularly with regard to interspecies studies and comparability [31]. Hence, the present study reveals crucial results for histologic and radiologic airway measurement, especially in the context of further development of radiologic methods.

### **Acknowledgements**

We thank Mrs. Silke Mitschke from the Institute of Pathology, University Medical Center of the Johannes Gutenberg University of Mainz, Germany for the excellent technical support. We also thank Mr. Dipl.-Phy. Hermann Götz for his technical support in dealing with the MicroCT scanner.

### **Funding**

This study was supported by the German Research Foundation (Deutsche Forschungsgemeinschaft – DFG, WE 4691/2-1).

### **Declaration of interest**

None

## References

1. Gamble G, Beaumont B, Smith H, Zorn J, Sanders G, Merrilees M, MacMahon S, Sharpe N. B-mode ultrasound images of the carotid artery wall: correlation of ultrasound with histological measurements. *Atherosclerosis* 1993; 102(2): 163-173.
2. Wong M, Edelstein J, Wollman J, Bond MG. Ultrasonic-pathological comparison of the human arterial wall. Verification of intima-media thickness. *Arterioscler Thromb* 1993; 13(4): 482-486.
3. Choi SM, Choi DK, Kim TH, Jeong BC, Seo SI, Jeon SS, Lee HM, Choi H-Y, Jeon HG. A Comparison of Radiologic Tumor Volume and Pathologic Tumor Volume in Renal Cell Carcinoma (RCC). *PLoS One* 2015; 10(3): e0122019.
4. Alicioglu B, Kaplan M, Yurut-Caloglu V, Usta U, Levent S. Radiographic size versus surgical size of renal masses: which is the true size of the tumor? *J BUON* 2009; 14(2): 235-238.
5. Lee SE, Lee WK, Kim DS, Doo SH, Park HZ, Yoon CY, Hwang SI, Lee HJ, Choe G, Hong SK. Comparison of radiographic and pathologic sizes of renal tumors. *World J Urol* 2010; 28(3): 263-267.
6. Jeffery NN, Douek N, Guo DY, Patel MI. Discrepancy between radiological and pathological size of renal masses. *BMC Urol* 2011; 11: 2.
7. Schlomer B, Figenshau RS, Yan Y, Bhayani SB. How does the radiographic size of a renal mass compare with the pathologic size? *Urology* 2006; 68(2): 292-295.
8. Sluimer I, Schilham A, Prokop M, van Ginneken B. Computer analysis of computed tomography scans of the lung: a survey. *IEEE Trans Med Imaging* 2006; 25(4): 385-405.
9. Xu Z, Bagci U, Foster B, Mansoor A, Mollura DJ. Spatially constrained random walk approach for accurate estimation of airway wall surfaces. *Med Image Comput Comput Assist Interv* 2013; 16(Pt 2): 559-566.
10. Weinheimer O, Achenbach T, Bletz C, Duber C, Kauczor HU, Heussel CP. About objective 3-d analysis of airway geometry in computerized tomography. *IEEE Trans Med Imaging* 2008; 27(1): 64-74.
11. Kosciuch J, Krenke R, Gorska K, Zukowska M, Maskey-Warzechowska M, Chazan R. Relationship between airway wall thickness assessed by high-resolution computed tomography and lung function in patients with asthma and chronic obstructive pulmonary disease. *J Physiol Pharmacol* 2009; 60 Suppl 5: 71-76.
12. Nakano Y, Van Tho N, Yamada H, Osawa M, Nagao T. Radiological approach to asthma and COPD--the role of computed tomography. *Allergol Int* 2009; 58(3): 323-331.
13. Górska K, Krenke R, Kosciuch J, Korczynski P, Zukowska M, Domagala-Kulawik J, Maskey-Warzechowska M, Chazan R. Relationship between airway inflammation and remodeling in patients with asthma and chronic obstructive pulmonary disease. *Eur J Med Res* 2009; 14 Suppl 4: 90-96.
14. Estépar RSJ, Washko GG, Silverman EK, Reilly JJ, Kikinis R, Westin C-F. Accurate airway wall estimation using phase congruency. *Med Image Comput Comput Assist Interv* 2006; 9(Pt 2): 125-134.
15. Kosciuch J, Krenke R, Gorska K, Zukowska M, Maskey-Warzechowska M, Chazan R. Airway dimensions in asthma and COPD in high resolution computed tomography: can we see the difference? *Respir Care* 2013; 58(8): 1335-1342.
16. Bayat S, Porra L, Suhonen H, Janosi T, Strengell S, Habre W, Petak F, Hantos Z, Suortti P, Sovijärvi A. Imaging of lung function using synchrotron radiation computed tomography: what's new? *European journal of radiology* 2008; 68(3 Suppl): S78-83.
17. Kurashima K, Hoshi T, Takayanagi N, Takaku Y, Kagiya N, Ohta C, Fujimura M, Sugita Y. Airway dimensions and pulmonary function in chronic obstructive pulmonary disease and bronchial asthma. *Respirology* 2012; 17(1): 79-86.

18. Achenbach T, Weinheimer O, Biedermann A, Schmitt S, Freudenstein D, Goutham E, Kunz RP, Buhl R, Dueber C, Heussel CP. MDCT assessment of airway wall thickness in COPD patients using a new method: correlations with pulmonary function tests. *Eur Radiol* 2008; 18(12): 2731-2738.
19. Jobst BJ, Weinheimer O, Buschulte T, Trauth M, Tremper J, Delorme S, Becker N, Motsch E, Gross ML, Trotter A, Eichinger M, Kauczor HU, Wielputz MO. Longitudinal airway remodeling in active and past smokers in a lung cancer screening population. *Eur Radiol* 2019; 29(6): 2968-2980.
20. Konietzke P, Wielputz MO, Wagner WL, Wuennemann F, Kauczor HU, Heussel CP, Eichinger M, Eberhardt R, Gompelmann D, Weinheimer O. Quantitative CT detects progression in COPD patients with severe emphysema in a 3-month interval. *Eur Radiol* 2020.
21. Rodriguez A, Ranallo FN, Judy PF, Gierada DS, Fain SB. CT reconstruction techniques for improved accuracy of lung CT airway measurement. *Med Phys* 2014; 41(11): 111911.
22. Revel M-P, Faivre J-B, Remy-Jardin M, Deken V, Duhamel A, Marquette C-H, Tacelli N, Bakai A-M, Remy J. Automated lobar quantification of emphysema in patients with severe COPD. *Eur Radiol* 2008; 18(12): 2723-2730.
23. Ukil S, Reinhardt JM. Smoothing lung segmentation surfaces in three-dimensional X-ray CT images using anatomic guidance. *Acad Radiol* 2005; 12(12): 1502-1511.
24. Wielputz MO, Eichinger M, Weinheimer O, Ley S, Mall MA, Wiebel M, Bischoff A, Kauczor H-U, Heußel CP, Puderbach M. Automatic airway analysis on multidetector computed tomography in cystic fibrosis: correlation with pulmonary function testing. *J Thorac Imaging* 2013; 28(2): 104-113.
25. Wagner WL, Wuennemann F, Pacile S, Albers J, Arfelli F, Dreossi D, Biederer J, Konietzke P, Stiller W, Wielputz MO, Accardo A, Confalonieri M, Cova M, Lotz J, Alves F, Kauczor HU, Tromba G, Dullin C. Towards synchrotron phase-contrast lung imaging in patients - a proof-of-concept study on porcine lungs in a human-scale chest phantom. *Journal of synchrotron radiation* 2018; 25(Pt 6): 1827-1832.
26. Langheinrich AC, Bohle RM, Breithecker A, Lommel D, Rau WS. [Micro-computed tomography of the vasculature in parenchymal organs and lung alveoli]. *RoFo : Fortschritte auf dem Gebiete der Rontgenstrahlen und der Nuklearmedizin* 2004; 176(9): 1219-1225.
27. Sluimer I, Prokop M, van Ginneken B. Toward automated segmentation of the pathological lung in CT. *IEEE Trans Med Imaging* 2005; 24(8): 1025-1038.
28. West MJ. Tissue shrinkage and stereological studies. *Cold Spring Harb Protoc* 2013; 2013(3).
29. Salmhofer W, Rieger E, Soyer HP, Smolle J, Kerl H. Influence of skin tension and formalin fixation on sonographic measurement of tumor thickness. *J Am Acad Dermatol* 1996; 34(1): 34-39.
30. Abramson DH, Scheffler AC, Almeida D, Folberg R. Optic nerve tissue shrinkage during pathologic processing after enucleation for retinoblastoma. *Arch Ophthalmol* 2003; 121(1): 73-75.
31. Lum H, Mitzner W. Effects of 10% formalin fixation on fixed lung volume and lung tissue shrinkage. A comparison of eleven laboratory species. *Am Rev Respir Dis* 1985; 132(5): 1078-1083.
32. Sutinen S, Pääkko P, Lahti R. Post-mortem inflation, radiography, and fixation of human lungs. A method for radiological and pathological correlations and morphometric studies. *Scand J Respir Dis* 1979; 60(1): 29-35.
33. Forrest JB. Measurement of the volume shrinkage of lung tissue due to rapid freezing followed by freeze substitution. *J Physiol* 1969; 202(2): 108P+.

34. Carney DE, Bredenberg CE, Schiller HJ, Picone AL, McCann UG, Gatto LA, Bailey G, Fillinger M, Nieman GF. The mechanism of lung volume change during mechanical ventilation. *Am J Respir Crit Care Med* 1999; 160(5 Pt 1): 1697-1702.
35. Tsunoda S, Martin CJ. Lung tissue shrinkage after freeze substitution for histologic study. *Am Rev Respir Dis* 1973; 107(5): 876-878.
36. Fukaya H, Martin CJ. Lung tissue shrinkage for histologic preparations. *Am Rev Respir Dis* 1969; 99(6): 946-948.
37. Hoang DM, Voura EB, Zhang C, Fakri-Bouchet L, Wadghiri YZ. Evaluation of coils for imaging histological slides: signal-to-noise ratio and filling factor. *Magn Reson Med* 2014; 71(5): 1932-1943.
38. Thurlbeck WM. Post-mortem lung volumes. *Thorax* 1979; 34(6): 735-739.
39. Mazzone RW, Kornblau S, Durand CM. Shrinkage of lung after chemical fixation for analysis of pulmonary structure-function relations. *J Appl Physiol Respir Environ Exerc Physiol* 1980; 48(2): 382-385.
40. Schmitt C. Bronchialwandvermessung in der modernen Diagnostik - Vergleich histologischer und bildgebender Verfahren im Tierversuch. Springer Research, Wiesbaden, Germany, 2017.
41. Achenbach T, Weinheimer O, Brochhausen C, Hollemann D, Baumbach B, Scholz A, Düber C. Accuracy of automatic airway morphometry in computed tomography-correlation of radiological-pathological findings. *European journal of radiology* 2012; 81(1): 183-188.
42. Achenbach T, Weinheimer O, Dueber C, Heussel CP. Influence of pixel size on quantification of airway wall thickness in computed tomography. *J Comput Assist Tomogr* 2009; 33(5): 725-730.
43. Achenbach T, Weinheimer O, Buschsieweke C, Heussel CP, Thelen M, Kauczor HU. [Fully automatic detection and quantification of emphysema on thin section MD-CT of the chest by a new and dedicated software]. *RoFo : Fortschritte auf dem Gebiete der Rontgenstrahlen und der Nuklearmedizin* 2004; 176(10): 1409-1415.
44. Tinnemans JG, Wobbles T, Holland R, Hendriks JH, van der Sluis RF, Lubbers EJ, de Boer HH. Mammographic and histopathologic correlation of nonpalpable lesions of the breast and the reliability of frozen section diagnosis. *Surg Gynecol Obstet* 1987; 165(6): 523-529.
45. Wilson MW, Rodriguez-Galindo C, Billups C, Haik BG, Laningham F, Patay Z. Lack of correlation between the histologic and magnetic resonance imaging results of optic nerve involvement in eyes primarily enucleated for retinoblastoma. *Ophthalmology* 2009; 116(8): 1558-1563.
46. Bazot M, Nassar-Slaba J, Thomassin-Naggara I, Cortez A, Uzan S, Daraï E. MR imaging compared with intraoperative frozen-section examination for the diagnosis of adnexal tumors; correlation with final histology. *Eur Radiol* 2006; 16(12): 2687-2699.
47. Saito H, Kameda Y, Masui K, Murakami S, Kondo T, Ito H, Oshita F, Tsuboi M, Yokose T, Noda K, Nakayama H, Yamada K. Correlations between thin-section CT findings, histopathological and clinical findings of small pulmonary adenocarcinomas. *Lung Cancer* 2011; 71(2): 137-143.
48. Jiang B, Takashima S, Miyake C, Hakucho T, Takahashi Y, Morimoto D, Numasaki H, Nakanishi K, Tomita Y, Higashiyama M. Thin-section CT findings in peripheral lung cancer of 3 cm or smaller: are there any characteristic features for predicting tumor histology or do they depend only on tumor size? *Acta Radiol* 2014; 55(3): 302-308.
49. Lampen-Sachar K, Zhao B, Zheng J, Moskowitz CS, Schwartz LH, Zakowski MF, Rizvi NA, Kris MG, Ginsberg MS. Correlation between tumor measurement on Computed Tomography and resected specimen size in lung adenocarcinomas. *Lung Cancer* 2012; 75(3): 332-335.
50. Isaka T, Yokose T, Ito H, Imamura N, Watanabe M, Imai K, Nishii T, Woo T, Yamada K, Nakayama H, Masuda M. Comparison between CT tumor size and pathological

tumor size in frozen section examinations of lung adenocarcinoma. *Lung Cancer* 2014; 85(1): 40-46.

51. Goldstein NS, Soman A, Sacksner J. Disparate surgical margin lengths of colorectal resection specimens between in vivo and in vitro measurements. The effects of surgical resection and formalin fixation on organ shrinkage. *Am J Clin Pathol* 1999; 111(3): 349-351.

52. Noguchi M, Furuya S, Takeuchi T, Hirohashi S. Modified formalin and methanol fixation methods for molecular biological and morphological analyses. *Pathol Int* 1997; 47(10): 685-691.

53. Moelans CB, ter Hoeve N, van Ginkel J-W, ten Kate FJ, van Diest PJ. Formaldehyde substitute fixatives. Analysis of macroscopy, morphologic analysis, and immunohistochemical analysis. *Am J Clin Pathol* 2011; 136(4): 548-556.

54. Fox CH, Johnson FB, Whiting J, Roller PP. Formaldehyde fixation. *J Histochem Cytochem* 1985; 33(8): 845-853.

55. Gardner ES, Sumner WT, Cook JL. Predictable tissue shrinkage during frozen section histopathologic processing for Mohs micrographic surgery. *Dermatol Surg* 2001; 27(9): 813-818.

56. Kerns MJJ, Darst MA, Olsen TG, Fenster M, Hall P, Grevey S. Shrinkage of cutaneous specimens: formalin or other factors involved? *J Cutan Pathol* 2008; 35(12): 1093-1096.

57. Rieger J, Twardziok S, Huenigen H, Hirschberg RM, Plendl J. Porcine intestinal mast cells. Evaluation of different fixatives for histochemical staining techniques considering tissue shrinkage. *Eur J Histochem* 2013; 57(3): e21.

## Figure legends:

**Figure 1:** Depiction of the same bronchus with different imaging methods. Clear differences in resolution are present between CT (left) and MicroCT (middle) images. Detailed tissue illustration like differing between cartilage clasps or identifying ciliated epithelium is possible with light microscopy of histologic sections only (right, HE staining). CT pixel spacing 0.68 mm, MicroCT pixel spacing 0.02 mm, histologic section 20-fold magnitude.

**Figure 2:** Boxplots showing the bronchi wall thickness measurements of frozen and paraffin sections as well as in MicroCT and CT measurements using the integral based method (IBM) and the full-width-at-half-maximum method (FWHM). There was a significant difference between the groups. When histologic and computed tomographic measurements were compared, the scoring in paraffin sections and with MicroCT were closer than the evaluation via frozen section or CT. CT using FWHM revealed a high divergence to the other groups while CT using IBM were close to the results of the other imaging methods. The scale bar is scored in the measurement unit mm. [40]

**Figure 3:** Regression plots correlating the two histologic methods paraffin sections (top row) and frozen sections (bottom row) with the computertomographic measurements of Micro-CT (left line), CT using the integral based method (IBM, middle line) and CT using the full-width-at half-maximum method (FWHM, right line). R: Pearson's correlation

**Figure 4:** Regression plots of Micro-CT, CT using the integral based method (IBM) and CT using the full-width-at-half-maximum method (FWHM). R: Pearson's correlation

**Figure 5:** Bland Altman plots showing the distribution between paraffin sections (top row) or frozen sections (bottom row) with Micro-CT (left line), CT using the integral based method (IBM, middle line) and CT using the full-width-at-half-maximum method (FWHM, right line).

**Figure 6:** Bland Altman plots showing the distribution between Micro-CT, CT using the integral based method (IBM) and CT using the full-width-at-half-maximum method (FWHM).

## Tables and table legends:

**Table 1:** Results of the bronchus wall measurements of frozen and paraffin sections as well as MicroCT and CT measurements.

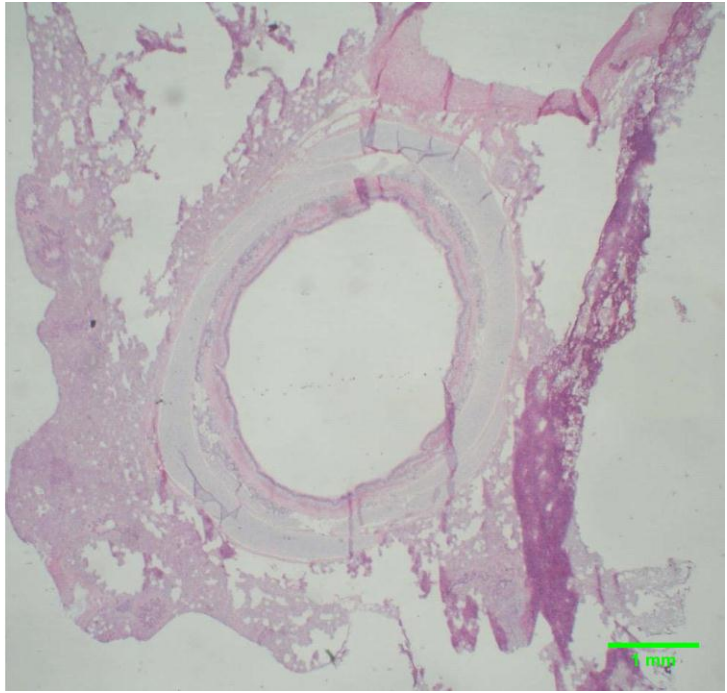
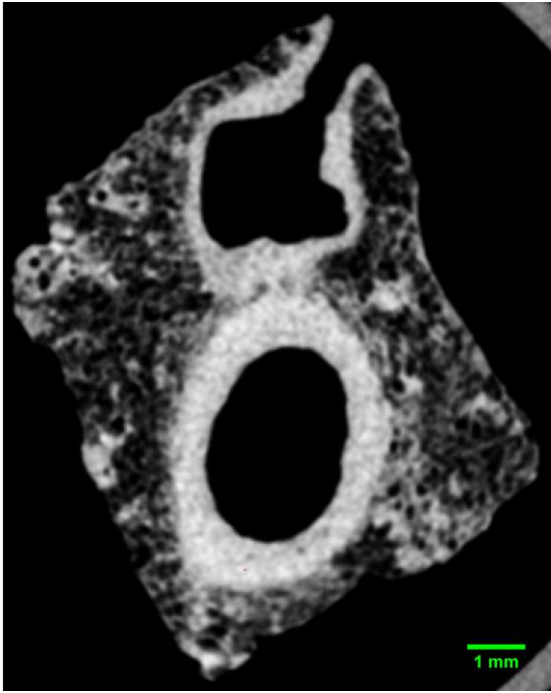
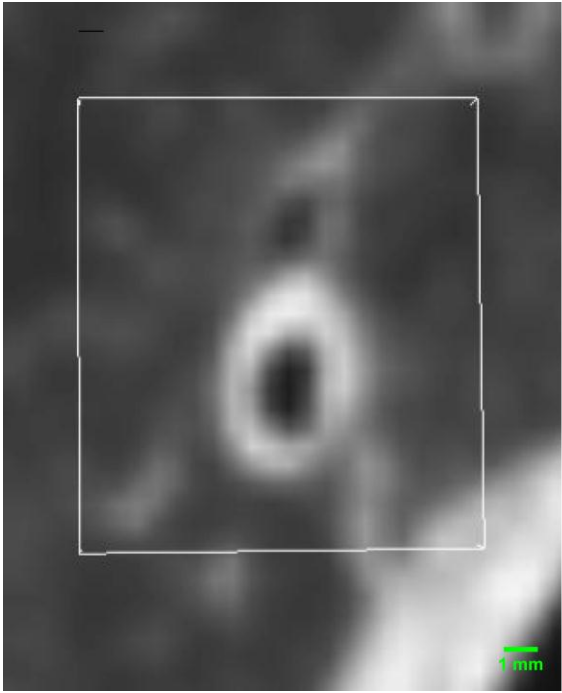
	Paraffin sections	Frozen sections	MicroCT	CT IBM	CT FWHM
N	7	7	7	7	7
Median	0.75	0.71	0.84	0.68	1.69
Mean value	0.75	0.66	0.82	0.72	1.64
Standard deviation	0.14	0.15	0.13	0.18	0.14
Minimum	0.05	0.42	0.56	0.43	1.36
Maximum	0.91	0.83	0.95	0.90	1.77
Percentiles	25	0.72	0.55	0.77	1.59
	75	0.91	0.76	0.90	1.75

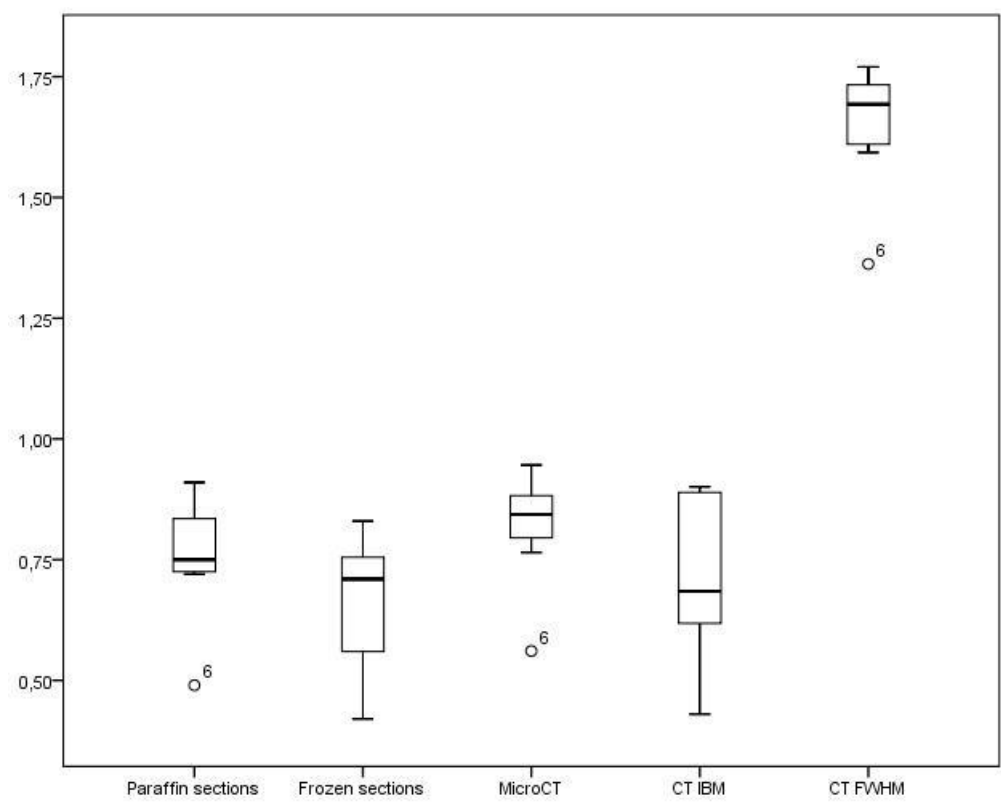
All values are given in the dimensional unit millimeters except for the count of evaluated bronchi (N). Partly according to [40].

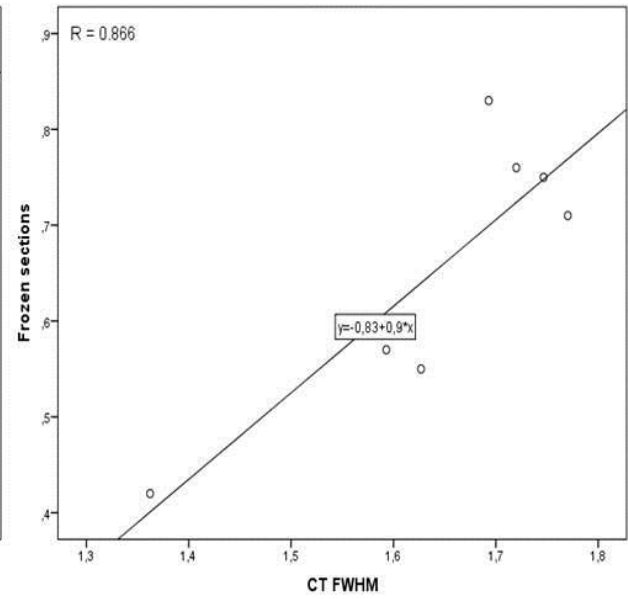
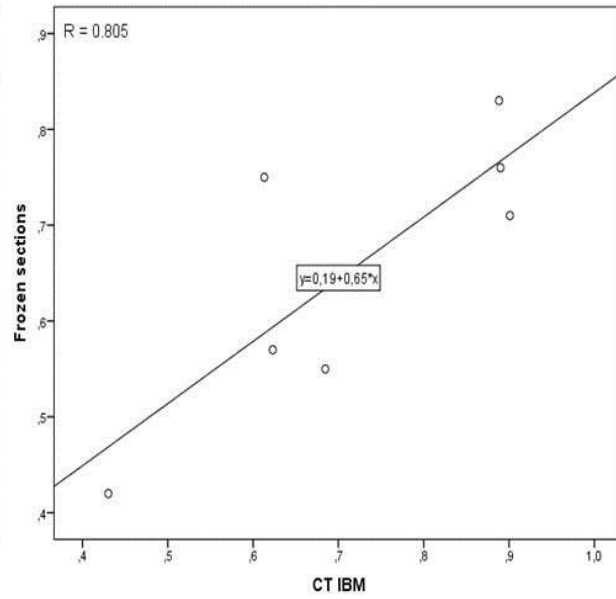
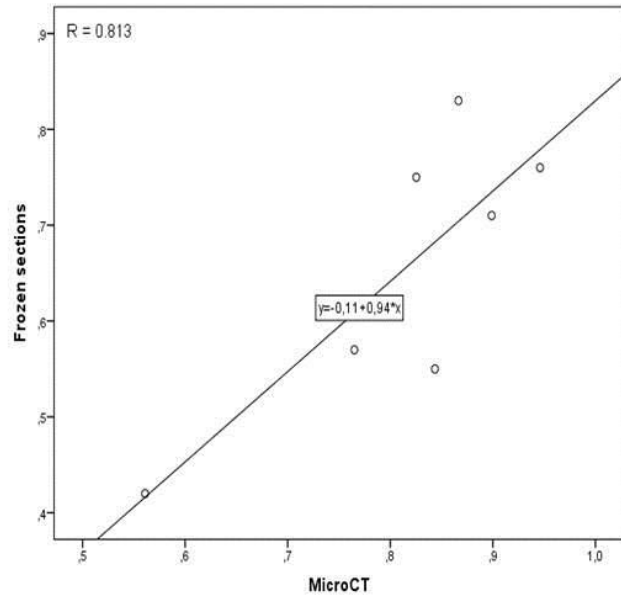
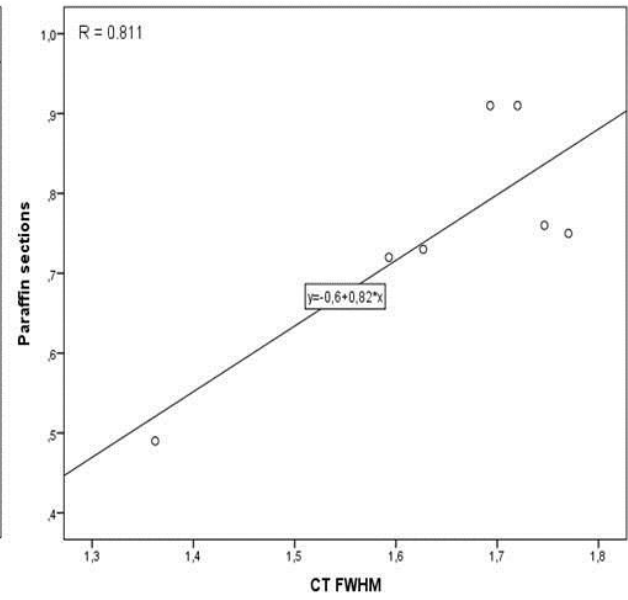
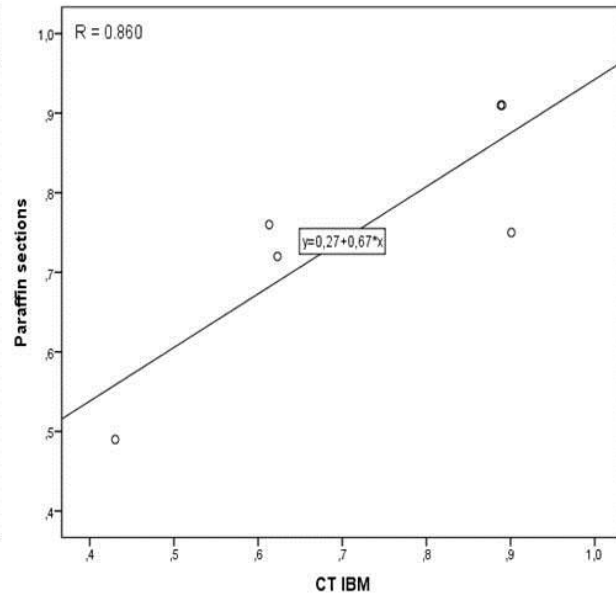
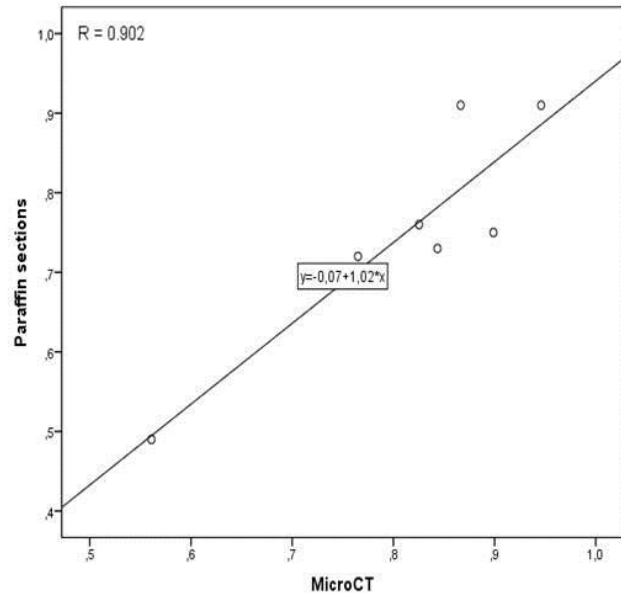
**Table 2.** Heat map showing Pearson's correlation among the investigated imaging modalities.

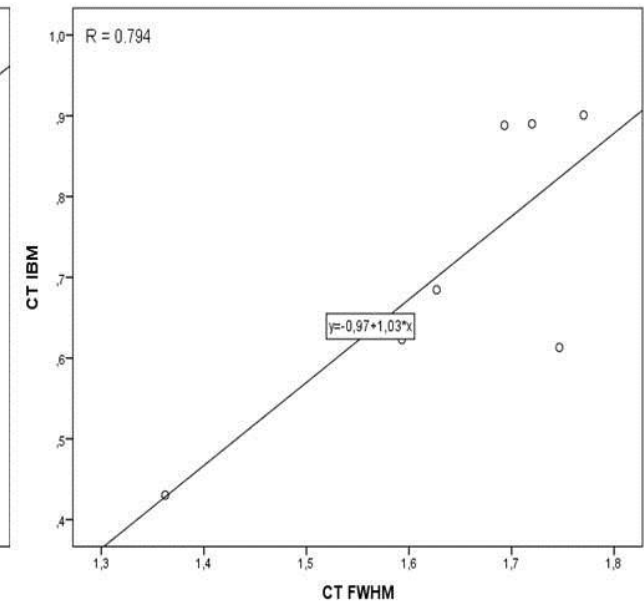
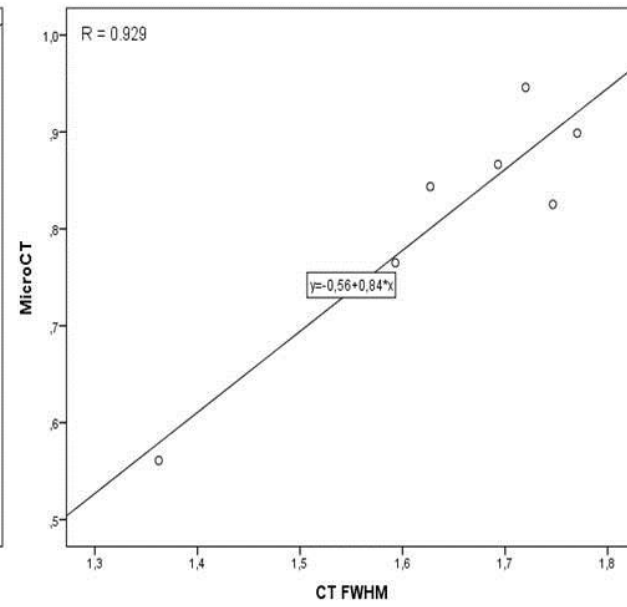
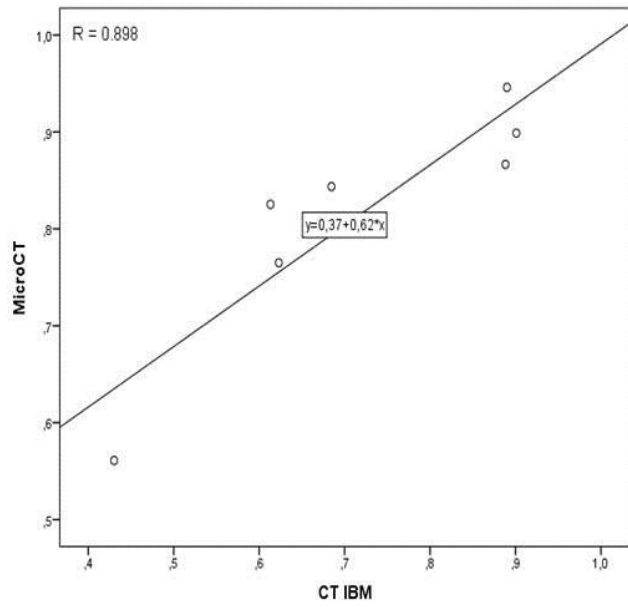
	Paraffin sections	Frozen sections	MicroCT	CT (IBM)	CT (FWHM)
Paraffin sections		0,902	0,902	0,86	0,811
Frozen sections	0,902		0,813	0,805	0,866
MicroCT	0,902	0,813		0,898	0,929
CT (IBM)	0,86	0,805	0,898		0,794
CT (FWHM)	0,811	0,866	0,929	0,794	

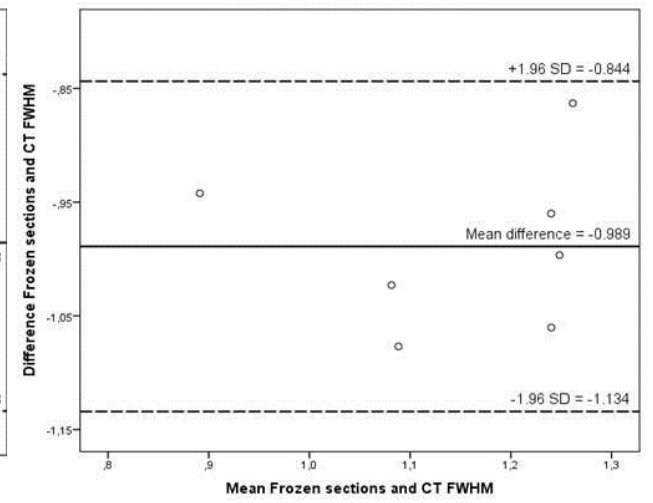
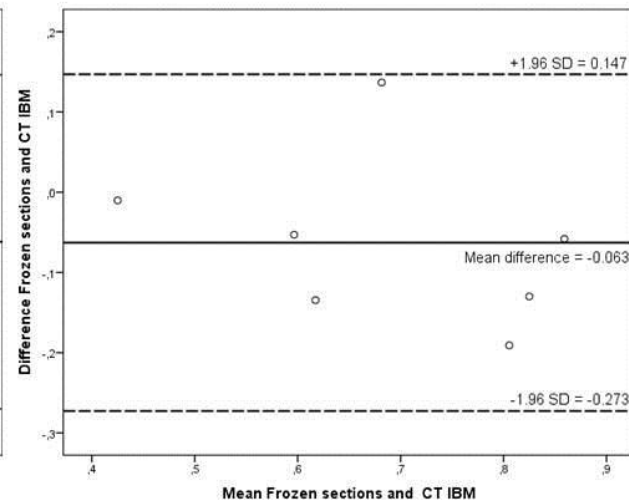
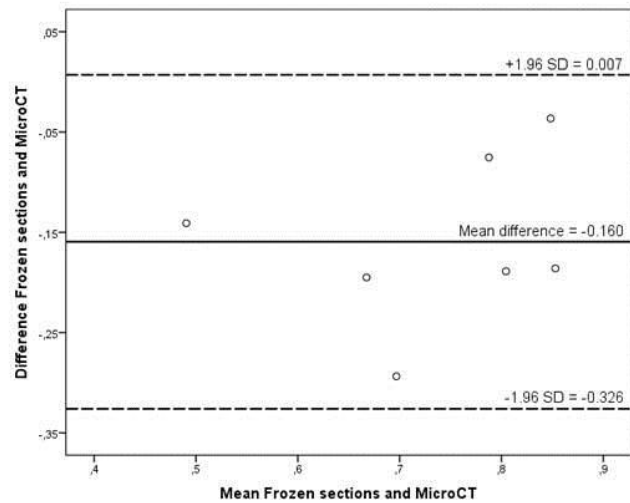
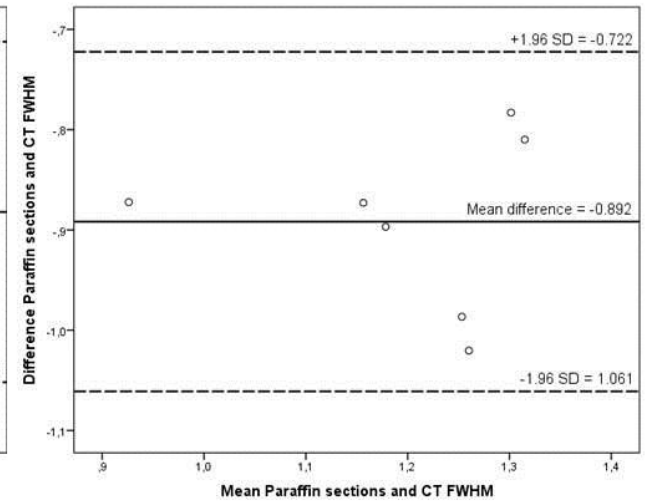
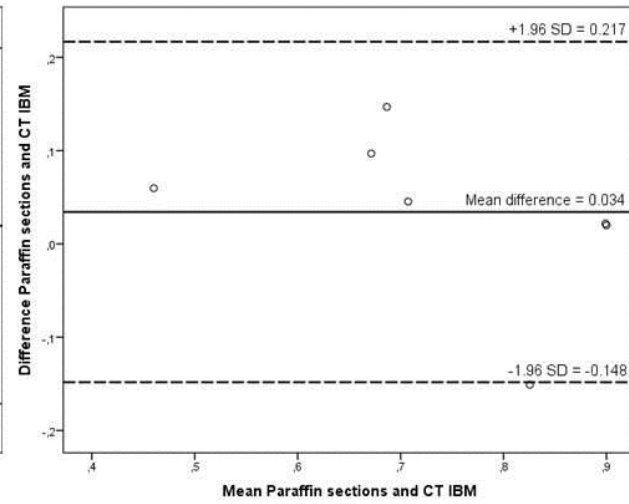
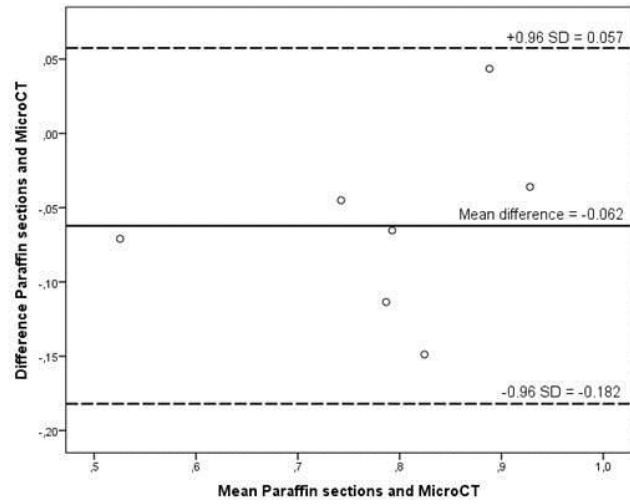
Highest correlation is given in intense red. Fading colour intensity with declining Pearson's correlation coefficient.

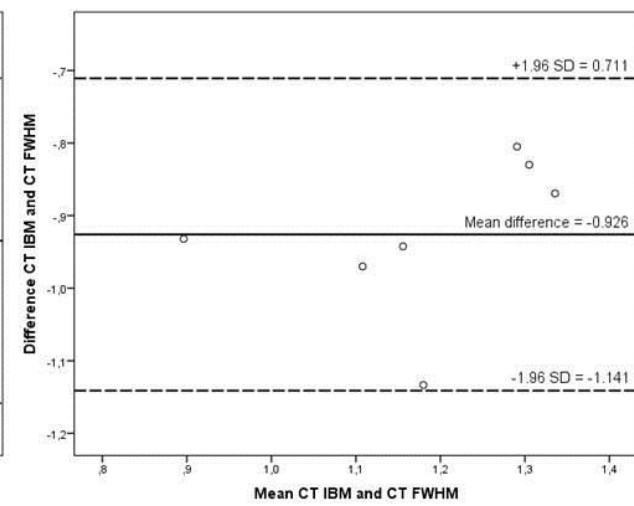
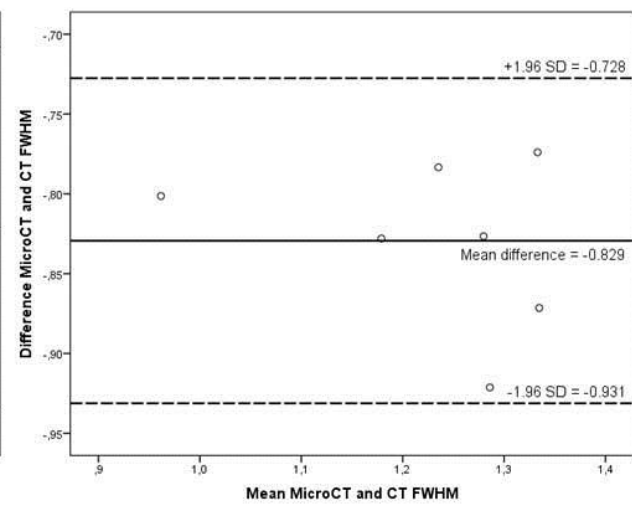
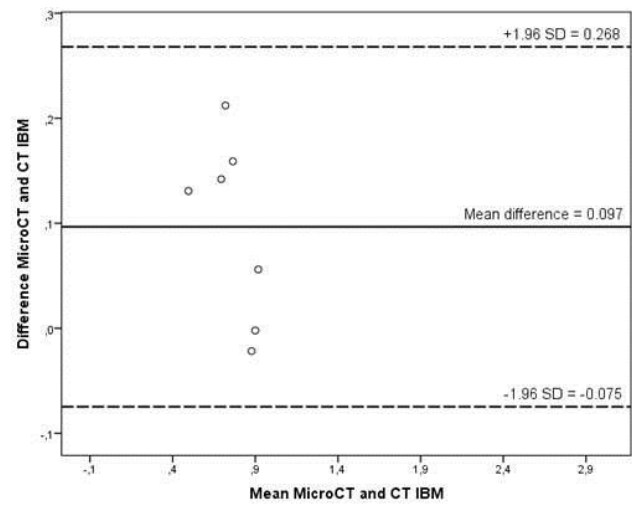












## Supplement

### Supplement figure legend

**Supplement Figure 1.** Regression plot and Bland Altman plot of paraffin and frozen sections showing the correlation as well as the distribution between the two histologic methods.

### Supplement Tables and Table legends

**Supplement Table 1:** Evaluation of statistical differences between the measurements among the investigated imaging modalities.

Test groups	p-value
Paraffin sections and Frozen sections	0.018
Paraffin sections and MicroCT	0.043
Paraffin sections and CT IBM	0.237
Paraffin sections and CT FWHM	0.018
Frozen sections and MicroCT	0.018
Frozen sections and CT IBM	0.176
Frozen sections and CT FWHM	0.018
MicroCT and CT IBM	0.063
MicroCT and CT FWHM	0.018
CT FWHM and CT IBM	0.018

Wilcoxon test with a significance level at  $p < 0.05$ . Partly according to [40].

**Supplement Table 2.** Pearson's correlation between the measurements among the investigated imaging modalities.

	R	95% confidence interval	Standard deviation	P-value
Paraffin sections and Frozen sections	0.902	0.638; 0.988	0.092	0.005
Paraffin sections and MicroCT	0.902	0.309; 0.997	0.193	0.005
Paraffin sections and CT (IBM)	0.860	0.291; 0.995	0.215	0.013
Paraffin sections and CT (FWHM)	0.811	-0.243; 0.989	0.378	0.027
Frozen sections and MicroCT	0.813	0.169; 0.994	0.221	0.026
Frozen sections and CT (IBM)	0.805	0.146; 0.987	0.252	0.029
Frozen sections and CT (FWHM)	0.866	0.240; 0.981	0.303	0.012
MicroCT and CT (IBM)	0.898	0.721; 0.988	0.066	0.006
MicroCT and CT (FWHM)	0.929	0.046; 0.994	0.241	0.003
CT (IBM) and CT (FWHM)	0.794	-0.151; 0.991	0.296	0.033

Linear regression analyses calculating Pearson's correlation coefficient with a significance level at  $P < 0.05$ .  $N = 7$ .  
R: Pearson's correlation.

**Supplement Table 3:** Mean differences of bronchus wall measurements between the investigated imaging methods.

	Paraffin sections	Frozen sections	MicroCT	CT IBM	CT FWHM
Paraffin sections mm (%)		0.09 (12.0)	0.07 (9.3)	0.03 (4.0)	0.89 (118.7)
Frozen sections mm (%)	0.09 (12.0)		0.16 (24.2)	0.06 (9.1)	0.98 (148.9)
MicroCT mm (%)	0.07 (9.3)	0.16 (24.2)		0.10 (12.2)	0.82 (100.0)
CT IBM mm (%)	0.03 (4.0)	0.06 (9.1)	0.10 (12.2)		0.92 (127.8)
CT FWHM mm (%)	0.89 (118.7)	0.98 (148.9)	0.82 (100.0)	0.92 (127.8)	

Mean differences of bronchus wall measurements between the investigated imaging methods in absolute (mm) and relative (% , brackets) values.

**Supplement Table 4:** Median differences of bronchus wall measurements between the investigated imaging methods.

	Paraffin sections	Frozen sections	MicroCT	CT IBM	CT FWHM
Paraffin sections mm (%)		0.04 (5.0)	0.09 (12.0)	0.07 (9.3)	0.94 (125.3)
Frozen sections mm (%)	0.04 (5.0)		0.13 (18.3)	0.03 (4.2)	0.98 (138.0)
MicroCT mm (%)	0.09 (12.0)	0.13 (18.3)		0.16 (19.0)	0.85 (101.2)
CT IBM mm (%)	0.07 (9.3)	0.03 (4.2)	0.16 (19.0)		1.01 (148.5)
CT FWHM mm (%)	0.94 (125.3)	0.98 (138.0)	0.85 (101.2)	1.01 (148.5)	

Median differences of bronchus wall measurements between the investigated imaging methods in absolute (mm) and relative (% , brackets) values.